Infrared lines as probes of solar magnetic features

III. Strong and weak magnetic fields in plages

I. Rüedi[1], S.K. Solanki[1], W. Livingston[2] and J.O. Stenflo[1]

[1] Institute of Astronomy, ETH-Zentrum, CH-8092 Zürich, Switzerland
[2] National Solar Observatory, NOAO*, P.O. Box 26732, Tucson, AZ 85726, USA

Abstract. Spectropolarimetric observations of solar plages in two infrared spectral lines (Fe I 15648.5Å and 15652.9Å) are analysed using synthetic profiles calculated in flux tube models. All the observed Stokes V profiles can be reproduced, in spite of the anomalous and complex shapes of many of them. The anomalous V profiles require 2 magnetic components to be properly fit. The most reliably derived parameter is the field strength B at a fixed height $z = 0$ in the atmosphere, corresponding to the $\tau_{5000} = 1$ level in the quiet sun. In the majority of the cases $B(z = 0)$ is determined with an accuracy of 20–50G. The measured $B(z = 0)$ values range between 400G and 1700G. The weakest measured $B(z = 0)$ are well below previously determined values, but are still limited by the Zeeman sensitivity of the $1.5\,\mu$m lines. We find that strong fields occur over the whole range of fluxes present in our sample, while weak fields are found only in patches of relatively small flux. Approximately 90% of the total magnetic flux in our sample is estimated to be in strong-field form, which is in good agreement with the results of Howard & Stenflo (1972) and Frazier & Stenflo (1972). The present results are shown to be compatible with magnetic measurements in the visible and with other recent infrared measurements. The importance of high spectral resolution for the reliable determination of weak fields is demonstrated. Finally, some of the consequences of the present work are discussed. For example, stringent limits are set on the amount of return flux in small magnetic flux tubes: If all tubes have some return flux in weak-field form, then it must be less than 5% of the flux of the dominant polarity. The weak-field components in general do not show any flows relative to the strong field. Thus most of the weak field patches were not undergoing convective collapse at the time of observation. This supports the existence of relatively stable weak-field features, such as the U-loops proposed by Spruit et al. (1987).

Key words: solar magnetic fields – solar faculae – magnetic flux tubes – infrared radiation – polarimetry

---

1. Introduction

The intrinsic strength B of the magnetic field in small-scale solar magnetic features has often been measured (e.g. Stenflo 1973; Harvey & Hall 1975; Tarbell & Title 1977; Frazier & Stenflo 1978; Wiehr 1978; Brault & Noyes 1983; Solanki & Stenflo 1984; Stenflo & Harvey 1985; Solanki et al. 1987; Stenflo et al. 1987b; Deming et al. 1988; Zirin & Popp 1989; Zayer et al. 1989, 1990; Del Toro et al. 1990; Keller et al. 1990b; Rabin 1992) and it is now accepted by most researchers that a major fraction of the solar magnetic flux is in the form of kG fields in the lower and middle photosphere (Howard & Stenflo 1972; Frazier & Stenflo 1972, cf. reviews by Stenflo 1989; Solanki 1990, 1992), but see Semel (1986) and Zirin (1988) for dissenting views. At present it is still unclear whether a truly weak component of the magnetic field exists and, if it does, what fraction of the magnetic flux is in weak-field form. We call a field weak if its plasma $\beta > 1$, where $\beta = 8\pi P / B^2$, with P the gas pressure in the magnetic feature. Note that fields classified as weak according to the above definition need not be truly weak, it may still have a strength of 1 kG. Stenflo (1982), from Hanle effect measurements of turbulent fields, and Spruit et al. (1992) from CLV observations of intranetwork elements made by Martin (1988), have argued for the presence of a weak field, but these measurements are not conclusive.

A number of authors have argued against the dominance of strong fields. Zirin & Popp (1989) have argued from measurements of $12\,\mu$m lines, formed just below the temperature minimum region that the field strength is only 250–500G at all heights in the photosphere (cf. Zirin 1988). Semel (1986) has pointed out that it is possible to reproduce the Stokes V line ratio traditionally used to measure B with two magnetic components of opposite polarity, both having fields well below kG in strength (675G and 135G, respectively, both with the same filling factor). Finally, Del Toro et al. (1990) claim to have detected fields of well below kG strength in a large fraction of their observed features.

These investigations suggest the need to reconfirm the two-decade old results of Howard & Stenflo (1972) and Frazier & Stenflo (1972) using more sensitive diagnostics.

In the present paper we address the question of field strengths in solar faculae anew using observations of Fe I 15648.5Å, a Zeeman triplet with Landé factor $g = 3$, and Fe I 15652.9Å, with effective Landé factor $g_{\rm eff} = 1.53$. These spectral lines have been amply described by Solanki et al. (1992a, henceforth called

Paper II), where their manifold advantages over the normally used high-g lines in the visible for the present undertaking have also been discussed. Together they can not only detect patches of weak fields better than visible lines, but can also determine their field strengths down to approximately 400–500G.

However, before they can be applied to reliably determine the field strength the eye-catchingly anomalous shapes of some of the observed Stokes V profiles of the $g = 3$ line must be explained within the context of the generally used flux tube models of magnetic features. The explanation of these anomalous profiles is another of the main aims of the present paper.

A summary of some preliminary results of the present investigation has been given by Solanki et al. (1992c).

2. Observational data

The observations analysed in the present paper were obtained during 1990 in the course of three observing runs with the vertical grating spectrograph of the McMath solar telescope on Kitt Peak and the "Baboquivari" infrared detector. The spatial resolution is estimated to lie between $3''$ and $5''$. More details on the data acquisition are to be found in Paper II and Livingston (1991). We analyse 27 Stokes I and V spectra of $\lambda15648\text{Å}$ and $\lambda15652\text{Å}$ obtained in various active region plages. This data set is a subset of approximately 200 spectra of solar plages observed near disk centre. In the present paper we prefer to restrict ourselves to a limited number of line profiles, so that we can expend a greater effort on reproducing the shapes of the observed profiles using synthetic Stokes profiles calculated numerically in flux tube models. This approach allows us to obtain physical parameters of more direct relevance to the physical understanding of the magnetic features than a simpler analysis, such as that of Rabin (1992), which, on the other hand, covers a larger number of spectra. The analysed profiles have been chosen from the full data set according to the following criteria:

1. The spatial resolution element should not contain any obvious pores.

2. The observed regions should be sufficiently far from sunspots, so that seeing does not smear any signal from the penumbra into the observed Stokes V.

3. Approximately two thirds of the chosen spectra have Stokes V profiles which appear "simple" or "normal" to the eye, while the rest are obviously anomalous or "complex". This ratio corresponds roughly to that of the whole data set. However, the binning of spectra into simple and complex ones is far from clear-cut for a number of spectra and a measure of subjectivity cannot be avoided in these cases.

The meaning of "simple" and "complex" spectra becomes clear upon inspecting Figs. 1–8. Consider for the moment only the observed spectra, i.e. the solid curves in Fig. 1a–8a. In Figs. 1a, 2a and 3a three "normal" Stokes V spectra are shown, i.e. each of the two σ-components of each spectral line is smooth with a single peak, and the V profiles of the $g = 3$ line are relatively antisymmetric. Upon a cursory inspection each of these profiles seems to result from regions with a single magnetic component. However, as we shall see in Sect. 3.1 this is not always the case. A profile that appears simple need not always represent a simple magnetic structure.

The profiles in Figs. 4a–8a are anomalous or complex in the sense that the presence of more than one magnetic or velocity component is fairly obvious. This is particularly true for the

$g = 3$ line. The profile shown in Fig. 6a is a border-line case in which noise may possibly mimic the signature of a second field component, although the statistical probability that noise is the cause is extremely small. The profile analysed by Zayer et al. (1989) is another example of a border-line case between normal and anomalous profiles.

Among the "anomalous" profiles we have tried to sample a variety of Stokes V profile shapes, since it is our aim to see if and under what conditions the anomalous profiles can be reproduced using traditional flux tube models of the magnetic field.

3. Method of analysis and modelling

To derive magnetic and, to a more limited extent, thermodynamic information from the spectra we reproduce the observed Stokes V profiles as well as possible with synthetic V profiles calculated along multiple rays in model flux tubes that satisfy exact pressure balance in the thin-tube approximation. The flux tube models and the radiative transfer through them has been described in Sect. 2 of Paper II. The atmospheres used to model the gas in the magnetic features and in their surroundings have also been described in Paper II. The two (flux tube) atmospheres which provide the best fits to the observations analysed in this paper are the HSRASP (originally an atmosphere describing the quiet sun) and PLA (a flux tube model for active region plage flux tubes).

In addition to using flux tube models we initially also fit the majority of the spectra with models possessing height-independent fields. In agreement with Zayer et al. (1989) such models are unable to reproduce the widths of the σ-components of the $g = 3$ line unless numerous magnetic components, each with a slightly different field strength and its own filling factor f, are introduced. With such a horizontal distribution of field strengths all the profiles can be reproduced, if additionally the Stokes V profiles are broadened by a macroturbulence of 2km s^{-1} (cf. Zayer et al. 1989). For the normal profiles the field strength distribution has a peak close to the value of B derived from the peak separation of Stokes V and a spread of approximately 500G. Only symmetric distributions of a simple form, e.g. $f(B)$ decreasing linearly or quadratically with B on both sides of the B with the largest f, have been used to model the simple spectra. Although successful, such vertically constant fields have some major disadvantages. 1. The number of free parameters is large and the physical insight gained from such fits is relatively small. 2. Physical confinement mechanisms require that the field strength changes with height (e.g. Spruit 1976, Deinzer et al. 1984, Steiner et al. 1986). 3. Zayer et al. (1989) were unable to reproduce visible and infrared lines simultaneously using a vertically constant field, but were successful when using a flux-tube model. In view of these disadvantages and problems we concentrate in the following on fits using the flux tube models described above. See Rüedi (1991) for more details on the fits based on height-independent field strengths.

Using synthetic profiles obtained from flux tube models we have first attempted to reproduce all profiles with a single magnetic component, i.e. a single flux tube. Only after we have been unable to fit the observed profiles in a satisfactory manner have we introduced a second magnetic component, i.e. a second flux tube with another field strength. For most of the "normal" profiles a single magnetic component is sufficient (examples and exceptions are discussed in Sect. 4), while for the anomalous Stokes
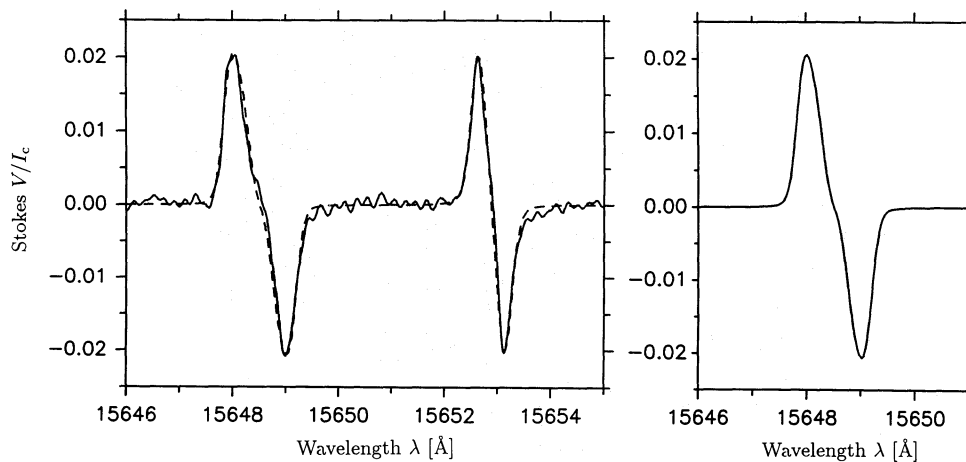
Fig. 1. a. Observed (solid) and synthetic (dashed) "normal" Stokes V profiles of Fe I 15648.5Å ($g = 3$) and Fe I 15652.9Å ($g_{\rm eff} = 1.53$). A model composed of a single thin magnetic flux tube with $B(z = 0) = 1520$G can reproduce the data. **b.** Calculated profile of the $g = 3$ line
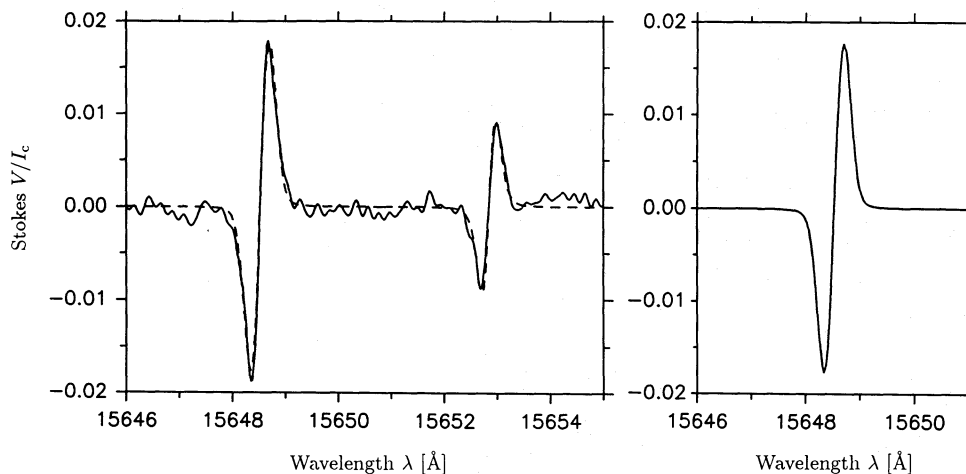
**Fig. 2.** Same as Fig. 1, but for a weak-field region with $B(z = 0) = 750$G
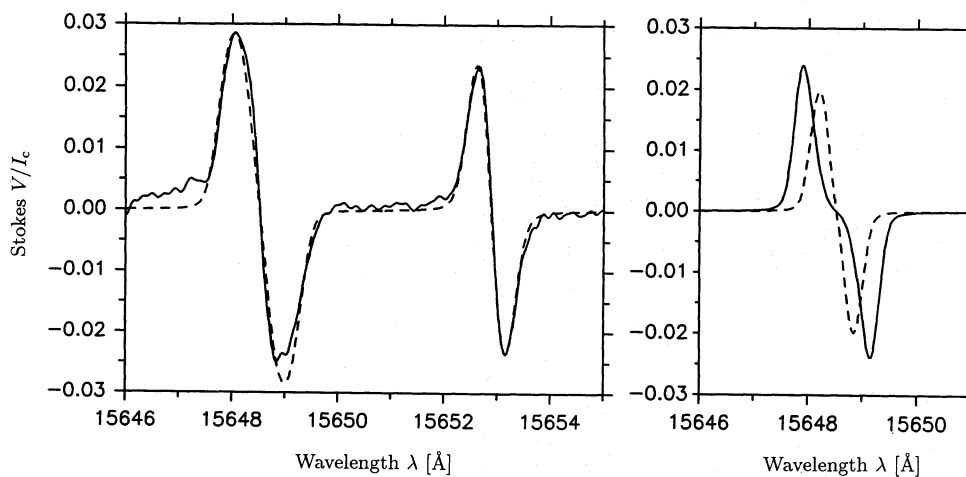
Fig. 3. a. Same as Fig. 1, but for a Stokes V spectrum in which the $g = 3$ line has abnormally broad σ-components, so that two flux-tube components of the same polarity, with $B_1(z = 0) = 1600$G and $B_2(z = 0) = 1180$G, respectively, are required to reproduce it. **b.** The synthetic Stokes V profiles of the $g = 3$ line resulting from each of the two individual flux-tube components. Solid curve: $B_1(z = 0) = 1600$G, dashed curve: $B_2(z = 0) = 1180$G

V profiles two components are always required. The total number of free parameters for fits involving a single magnetic component is 4: two magnetic parameters, the field strength $B(z = 0)$ and the filling factor $\alpha(z = 0)$, as well as two thermodynamic parameters, a macroturbulent velocity $\xi_{\rm mac}$ and the temperature. The choice of temperature stratification is restricted to the empirical models described in Paper II. Due to the temperature insensitivity of the lines we do not require a finer grid in the present investigation. With these free parameters we fit the profile shapes and amplitudes of both lines simultaneously. Thus the present technique is similar to that of Zayer et al. (1989), except that we additionally fit the ratios between the Stokes V profiles of the two lines, which gives us a crude diagnostic of the temperature, as well as a constraint on the weaker fields (cf. Paper II).

When reproducing anomalous or complex profiles there are 7 free parameters in all: $B_1(z = 0)$ and $B_2(z = 0)$, the field strengths in the two components, $\alpha_1(z = 0)$ and $\alpha_2(z = 0)$, the filling factors in both components, $\Delta\lambda_V$, a relative flow velocity between the two magnetic components (assumed to be height independent, so that it only produces a relative shift between the V profiles
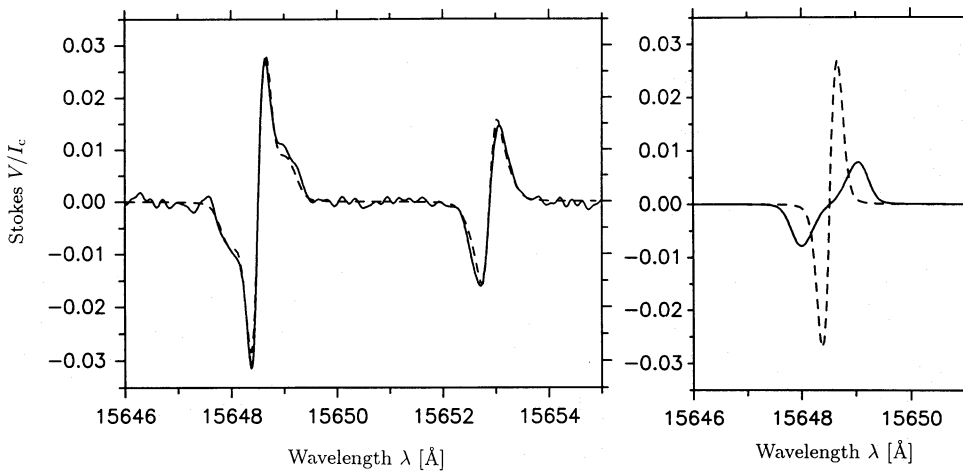
Fig. 4. Same as Fig. 3, but for a spectrum with a humped $g = 3$ line. The dashed curve in Fig. 4a is a sum of two Stokes V profiles (shown individually in Fig. 4b) calculated for $B_1(z = 0) = 1500$G and $B_2(z = 0) = 500$G, respectively

resulting from the two components)and finally a single macroturbulence ξ_{mac} and a single temperature model for both lines and both components. In some cases in which both components were sufficiently distinct we have also tried fitting the profiles with two ξ_{mac} and temperature components, but have found these added degrees of freedom to be unnecessary. Furthermore, although the $g = 3$ line is usually sufficiently split to allow the profiles due to two magnetic components to be distinguished, this is seldom the case for the $g_{eff} = 1.53$ line. Therefore we often do not have sufficient diagnostic information to constrain different temperatures and ξ_{mac} for the two components accurately.

4. Results: profile fits

We have been able to reproduce all profiles with at the most 2 magnetic flux tube components. In Figs. 1a–8a (left-hand frames) a selection of the observed profiles after Fourier smoothing (solid curves) and the best fits to them (dashed curves) are plotted. Both lines are shown. The $g = 3$ line at $\lambda 15648.5$Å is easily recognisable by its larger splitting. In Figs. 1b–8b (right-hand frames) calculated profiles of each magnetic component of the $g = 3$ line are shown. If only a single magnetic component is required to fit the observations then the profile in the right-hand frame corresponds to the best fit profile. If two magnetic components are required then the best-fit profile is the sum of the solid and dashed profiles in the right-hand frame. Let us now briefly discuss the individual spectra.

4.1. Discussion of individual profiles

Figure 1 shows a typical normal profile (spectrum No. 6 in Table 1. See Sect. 5 for a discussion of the Table). We have been able to reproduce it with a single flux tube component having $B(z = 0) = 1520$G and an internal temperature structure corresponding to the PLA model (see Paper II for a description of this model). Note that not only do we reproduce the profile shapes of the two lines, but also their ratio. Note how the widths of the σ-components are well reproduced without requiring any additional magnetic broadening.

As a second example we plot in Fig. 2 another simple profile (spectrum No. 15). It is evident that the field strength is lower than in region 6 (Fig. 1): The peak separation in this case gives 580 G, compared to 1425 G for spectrum No. 6. Note also the correspondingly smaller σ-component widths of the $g = 3$

line, as well as the much larger ratio between the Stokes V peaks of the $g = 3$ line to the $g_{eff} = 1.53$ line. The profiles of spectrum No. 15 are fit by a flux tube with $B(z = 0) = 750$G. The narrower σ-components and most of the increase of the line ratio automatically result from the lower $B(z = 0)$ (cf. Paper II). A minor part of the difference of the line ratio is due to a slightly lower temperature in the flux tubes giving rise to spectrum 15 (for the best fit the HSRASP model was used).

In Fig. 3 we have plotted a spectrum (No. 17) which looks relatively normal and at first sight suggests a single magnetic component. However, fits with such a model showed that the calculated Stokes V profiles, particularly that of the $g = 3$ line, have much too narrow σ-components. Thus additional magnetic broadening is required, which we introduce by adding a second magnetic flux tube component. The fit shown in Fig. 3a is composed of two such components with $B_1(z = 0) = 1600$G (solid profile in Fig. 3b) and $B_2(z = 0) = 1180$G (dashed profile in Fig. 3b). Both components of the field have the same polarity.

Due to the smooth shapes of the measured σ-components it is not possible to rule out that more than two magnetic components are present. For example, if we assume a distribution of height-independent field strengths $f(B)$ to reproduce this profile, then the distribution is single peaked, although very broad, with a FWHM $\gtrsim 1500$ G.[1] In principle a very large vertical gradient in B could also account for the anomalous σ-component width of profile No. 17. However, it is difficult to envisage how the field-strength gradient could be so different from that in other regions without affecting the atmosphere in an easily visible manner (e.g. by *large* temperature changes). For most of the observed profiles there is generally not much room for significant additional magnetic broadening beyond that provided by one (Figs. 1 and 2) or two thin magnetic flux tubes (Figs. 4–8). We therefore see no cause to abandon our simple interpretation based on two flux-tube components. If the field strengths of both components are sufficiently similar then the σ-components of the resulting Stokes V profile show anomalous broadening, as in Fig. 3. If they are further apart, then the 2 components become individually visible in the profile of the $g = 3$ line, as in Fig. 4 (below).

The profiles plotted in Fig. 4 (spectrum No. 20) are reproduced by two magnetic components with $B_1(z = 0) = 1500$G and $B_2(z = 0) = 500$G, i.e. again only a single polarity, but with a much larger difference in the $B(z = 0)$ of the two components

---

[1] A height-independent field is however not physically so realistic.
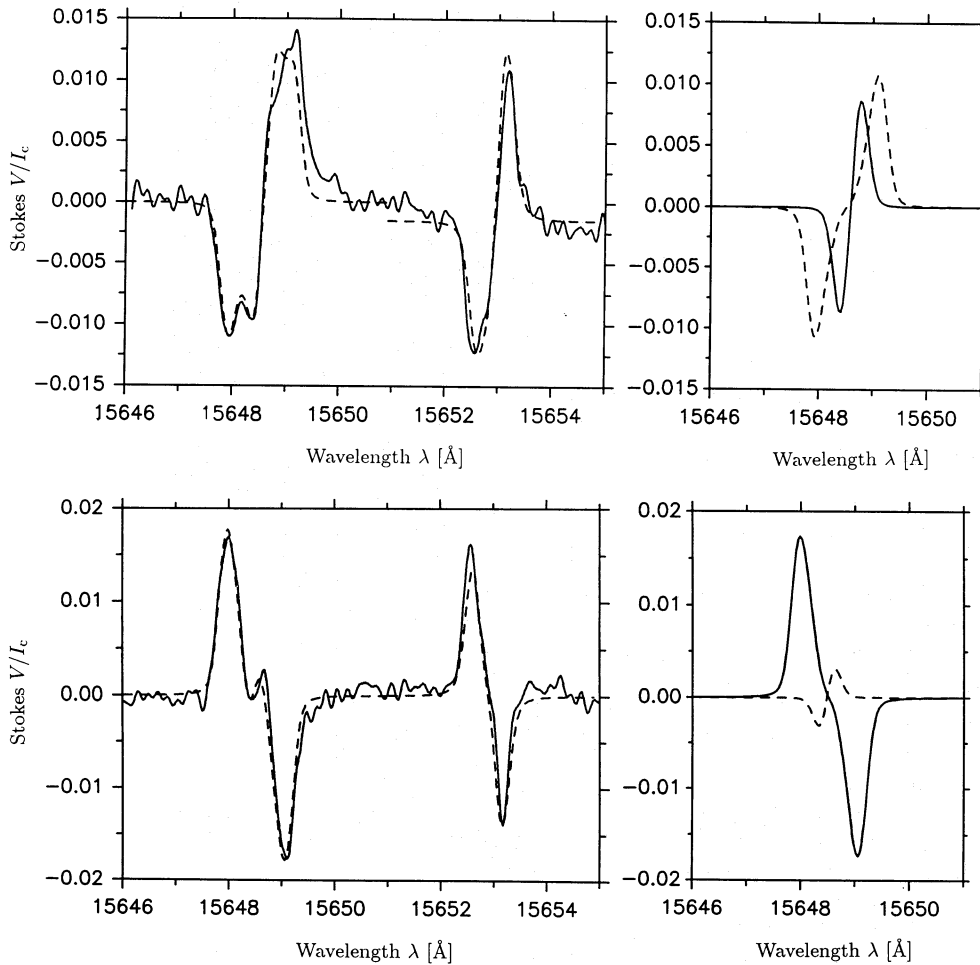
Fig. 5. Same as Fig. 3, but for asymmetric Stokes V profiles. The dashed curve in Fig. 4a results for $B_1(z = 0) = 1550$G, $B_2(z = 0) = 800$G and a wavelength shift $\Delta\lambda_V$ between the two components corresponding to 1.4km s^{-1}

Fig. 6. Same as Fig. 3, but for a $g = 3$ line with a weak inversion at its core. $B_1(z = 0) = 1500$g, $B_2(z = 0) = -600$G (the negative sign signifies that the polarity is opposite to that of the strong field) and a $\Delta\lambda_V = 0.7$km s^{-1}

than in spectrum No. 17. The atmosphere is the HSRASP. The larger ratio of the field strengths (in combination with the smaller filling factor of the stronger B component) results in the 'hump' in the profile of the $g = 3$ line, a tell-tale sign of the presence of two distinct magnetic components. The Zeeman sensitivity of the $g_{\rm eff} = 1.53$ line is too small, so that its σ-components only get broadened.

All profiles discussed so far were antisymmetric within the limits set by noise and instrumental cross-talk. In Fig. 5 we show a spectrum in which the Stokes V profiles of both lines are obviously asymmetric (No. 22). This asymmetry differs from that seen in lines in the visible (e.g. Solanki & Stenflo 1984, 1985) or in infrared lines with smaller g (Muglach and Solanki 1992, which is Paper I of the present series) in that although the blue and red lobes of Stokes V have different shapes and amplitudes their areas are almost the same. Therefore, a line-of-sight velocity *gradient* (Illing et al. 1975; Solanki & Pahlke 1988) does not appear to be the main cause of the asymmetry.[2] Similarly, instrumental cross-talk from Stokes I, Q or U into V can be ruled out since it also primarily produces a significant blue-red *area* asymmetry (November 1991). On the other hand, we see no possibility of

producing the observed asymmetry without invoking any line-of-sight velocity at all.

The fit to the observed profiles shown in Fig. 5 which, although not perfect, does reproduce the main features of the profile, is based on two magnetic components of negative polarity, with $B_1(z = 0) = 1550$G and $B_2(z = 0) = 800$G. In addition the B_2 component is shifted relative to the B_1 component by 1.4 km s^{-1} towards the red.[3]

Consider now some of the profile shapes resulting when two opposite polarities are present within the resolution element. Figures 6, 7 and 8 show a sequence in which the flux in the minor polarity increases from a very small fraction of the dominant polarity flux in Fig. 6 to nearly the same amount in Fig. 8.

Although the amplitude of the secondary component in Fig. 6 (spectrum No. 24) lies at the 3σ level, its presence can easily be overlooked upon a cursory inspection and the profile falsely classified as a simple one. This profile illustrates the smallest signals visible in our data. The best fit to this spectrum is obtained with $B_1(z = 0) = 1500$G and $B_2(z = 0) = -600$G and a $\Delta\lambda_V = 0.7$km s^{-1} towards the red. However, due to the small S/N ratio

---

[2] However, this does not rule out the presence of longitudinal gradients, since, as demonstrated by Grossmann-Doerth et al. (1989), it requires extremely large changes in the velocity to produce a significant asymmetry in the $g = 3$ line due to its large Zeeman splitting.

[3] In a few of the observed spectra the zero-line of Stokes V showed a drift as a function of wavelength. Figure 5 is an example. In order to reproduce both profiles approximately correctly we have simply shifted the zero-level of the $g_{\rm eff} = 1.53$ line to match the approximate level of the continuum at its wavelength. We stress that the continuum offset cannot account for the observed asymmetry.
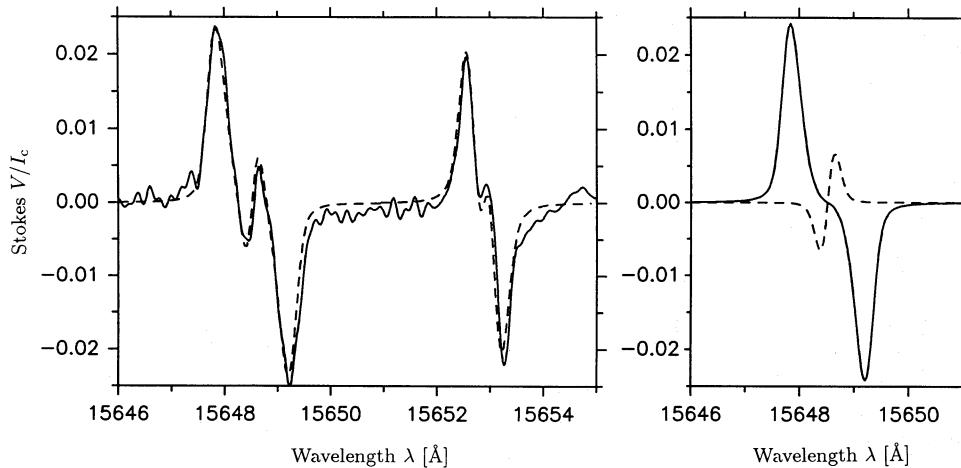
Fig. 7. Same as Fig. 6 for a $g = 3$ line with a stronger inversion. $B_1(z = 0) = 1650G$, $B_2(z = 0) = -600G$, $\Delta\lambda_V = 0$

of the second component its parameters are less certain than for other profiles. The profiles in Fig. 7 (spectrum No. 25) show much clearer signs of 2 magnetic components. The best-fit dashed curve in Fig. 7a was obtained with the following parameters: $B_1(z = 0) = 1650G$ and $B_2(z = 0) = -600G$. Finally, in Fig. 8 we show a spectrum (No. 26) in which the two magnetic components have almost equal strength and the V profile shows little resemblance to the classically expected form. The best fit in this case is achieved for $B_1(z = 0) = 1700G$ and $B_2(z = 0) = -1050G$. Note how the $g_{eff} = 1.53$ line reacts much less to the presence of a second component. In Figs. 6 and 7 it would be difficult to conclude on the presence of a second magnetic component just on the basis of this line. The difference in behaviour of the two lines is purely the result of their Landé factors. In Fig. 8 the second component is so strong that it is also clearly visible in the $g_{eff} = 1.53$ line. This concludes our overview of the different types of Stokes V profiles in our sample.

The presence of opposite polarities and of wavelength shifts between the two magnetic components can also lead to highly asymmetric Stokes V profiles (e.g. with 3 lobes, cf. Mathys 1988). Such profiles are studied in detail by Rüedi et al. (1992, Paper IV of the present series) and we do not consider them further here in order to avoid duplicating results.

4.2. Uniqueness of the fits

How unique are the parameters derived from the fits? For the profiles reproduced by a single component we feel reasonably confident in the uniqueness of the fits. We estimate that if $B(z = 0) \gtrsim 1300$ G, then it is accurate to within 15–30G if the S/N ratio is sufficient and the temperature structure used is the correct one. In slightly more than half the cases $B(z = 0)$ is determined with this accuracy. With decreasing $B(z = 0)$ its accuracy also decreases, until finally for a $B(z = 0) \lesssim 400G$–500G only an upper limit of 400–500G can be given (see Paper II). Since the temperature structure is not so well determined, the true uncertainty in $B(z = 0)$ is increased to approximately 25–50G in the best cases.

For the profiles requiring two magnetic components it is initially unclear whether other parameter combinations exist which reproduce the observations equally well. Consider, for example, Fig. 8. Instead of using two unshifted field components of different strengths and opposite polarity it is also possible to reproduce the $g = 3$ line with a combination of two Stokes V profiles of the same (negative) polarity and the same (small) field strength,

if they are shifted with respect to each other. Fig. 9a shows the same observed spectrum as Fig. 8, but with two magnetic components of the same polarity ($B_1(z = 0) = B_2(z = 0) = 900G$, $\Delta\lambda_V = 19$km s^{-1}). However, although the $g = 3$ line is reproduced excellently, the fit to the $g_{eff} = 1.53$ line is unacceptable. The reason is clear: Since the V peak separations in the fit shown in Fig. 8 (opposite polarities) are due to the different field strengths in the two components they scale with g (respectively g_{eff}) and are only half as large in the $g_{eff} = 1.53$ line. In Fig. 9b, on the other hand, the separation between the profiles of the two components is due to a velocity. This separation is independent of the Landé factor.

Similarly, we can rule out single polarity, 2-component fits to the profiles in Figs. 6 and 7. Also, the possibility of fitting the $g = 3$ line of spectrum No. 17 (Fig. 3) with a model having $B_1(z = 0) = B_2(z = 0) = 1400G$ and $\Delta\lambda_V \neq 0$ can be ruled out, since the resulting $g_{eff} = 1.53$ line is again too broad.

Could Stokes V profiles of a single magnetic component reproduce some of the complex observed profiles? We see only two possible ways for this to happen: Magnetooptical effects and a temperature inversion, e.g. due to a low-lying chromosphere. As discussed in Paper II even an inversion as minute as the one at the centre of the $g = 3$ line in Fig. 6 is difficult to explain with magnetooptical effects and larger inversions (such as the ones seen in Figs. 7 and 8) can certainly not be explained in this manner. Also, it is extremely unlikely that a temperature inversion, as produced by a chromosphere (e.g. Lites et al. 1987), is the correct explanation of the inversions seen in Figs. 6–8. Firstly, the 1.5 μm lines are sensitive to the temperature mainly in the lower photosphere (Paper I), so that any temperature inversion visible in their cores would have to occur in the lower or middle photosphere. It would therefore produce inversions in visible lines as well, which are not observed (Bruls & Solanki 1992). Secondly, a chromosphere should affect the cores of the $g = 3$ and $g_{eff} = 1.53$ lines almost equally, while the observed inversion is substantially stronger in the core of the $g = 3$ line in all cases, which is exactly what is expected if the inversion is due to an opposite polarity field.

We conclude from such tests and considerations that although it is often possible to reproduce the $g = 3$ line alone with different sets of parameters we have been able to find only a single (relatively noisy) case in which we could fit both line profiles equally well with two substantially different sets of model parameters. This point confirms once more the importance of measuring two lines with different g_{eff} in the infrared when studying small-scale
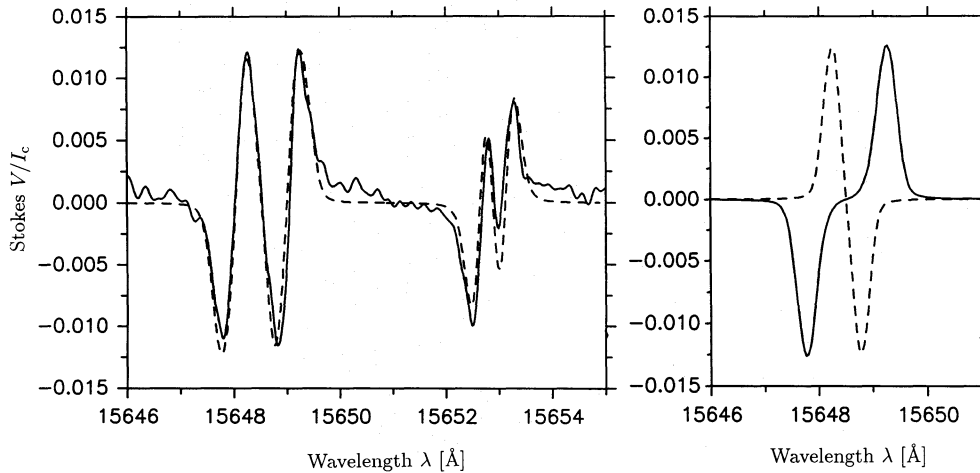
Fig. 8. Same as Fig. 6 for a very strong inversion. $B_1(z = 0) = 1700G$, $B_2(z = 0) = -1050G$, $\Delta\lambda_V = 0$

magnetic features. This point is equally valid for complex profiles observed in the visible (e.g. Skumanich & Lites 1991), where 2 lines with different g_{eff} also greatly enhance the uniqueness of the interpretation.

5. Results from the complete sample of analysed spectra

5.1. Overview

Parameters obtained directly from the line profiles or from the model fits are given in Table 1 for all the analysed spectra. Columns 1 and 2 give the spectrum number (quoted in Sect. 3) and the atmospheric model giving the best fit, respectively. In column 3 the field strength B derived from $\Delta\lambda_{max}$, the wavelength difference between the peaks of the red and blue lobes of Stokes V of the $g = 3$ line is listed. If a σ-component has more than one peak then $\Delta\lambda_{max}$ is measured between the highest ones. The $g = 3$ line in spectra 26 and 27 has 2 almost equally strong peaks in each σ-component, so that no unique value of B can be determined in this simple manner. As long as the $g = 3$ line is completely split B from $\Delta\lambda_{max}$ corresponds roughly to the field strength at the height of formation of the Stokes V maxima.[4] The rest of the parameters in Table 1 have been derived from flux tube fits. $B_i(z = 0)$ is the field strength at $z = 0$ which corresponds to $\tau_{5000} = 1$ in the average quiet sun. $B_i(\tau = 1)$ is the field strength at the $\tau_{5000} = 1$ level inside the flux tube. Subscripts $i = 1, 2$ refer to the first and second magnetic components, respectively, whereby $B_1 \geq B_2$. Note that the sign of B_2 reflects its polarity relative to the the first magnetic component. ξ_{mac} is the macroturbulent velocity, $\Delta\lambda_V$ is the wavelength shift (in velocity units) of the Stokes V profiles of component 2 relative to the profiles of component 1, $\beta = 8\pi P / B^2$ (P is the gas pressure within the magnetic feature), $\langle B \rangle$ is the field strength averaged over the spatial resolution element, and $\alpha(z = 0)$ is the magnetic filling factor at $z = 0$. A positive $\Delta\lambda_V$ implies that the gas in the weak-field component is flowing away from the observer relative to gas in the strong-field component (if we interpret the wavelength shift as a stationary flow). β is a measure of the energy density in the gas within the flux tube relative to that in the magnetic field. Roughly speaking a $\beta < 1$ signifies that the magnetic field dominates the energetics.

---

4   B from $\Delta\lambda_{max}$ generally corresponds to within 100G to the most common B of the horizontal B distributions derived from fits based on height-independent fields.

For spectrum No. 23 two almost equally good fits to both lines were obtained. Since we have no means of distinguishing between the two we have listed them both.

5.2. Field strengths

The $B(z = 0)$ in our sample range from 400G to 1700G, with a distinct bias towards larger field strength values. The smallest measured value of $B(z = 0)$ corresponds to the smallest $B(z = 0)$ that the $g = 3$ line can measure (Paper II). The largest measured value lies close to the largest $B(z = 0)$ that can be confined by the gas pressure of the field-free atmosphere ($\approx$ 1770G for the HSRASP, corresponding to a completely evacuated flux tube). No particular relationship is evident between the $B(z = 0)$ values of the two magnetic components contributing to a particular spectrum. $B_1(z = 0) - B_2(z = 0)$ ranges between 200G and 1050G. We estimate that 200G is, for the present data, the smallest measurable $B_1(z = 0) - B_2(z = 0)$. The field in component 2 does not appear to have any preferred polarity relative to component 1.

In Fig. 10a $B_1(z = 0)$ and $B_2(z = 0)$, together denoted by $B(z = 0)$ for simplicity, are plotted vs. $A_1(15648)$ and $A_2(15648)$, respectively (denoted by A(15648); it represents the average of the areas of the blue and red lobes of Stokes V for each magnetic component individually). $B(z = 0)$ values derived from one-magnetic-component fits are represented by circles, those obtained from two-magnetic-component fits by crosses. The straight line is a regression through all the strong-field data points. In the following we call fields with $\beta \leq 1$ strong ($\beta = 1$ corresponds to approximately $B(z = 0) = 1250G$, the exact value depends on the atmosphere within the flux tube), while fields with $\beta > 1$ are referred to as weak fields. The plotted line is almost identical to the regression line through only the strong-field circles. This suggests that the weak fields do not appear to affect the magnetic properties of the strong-field component. A(15648) is only a rough guide to the magnetic flux, or magnetic filling factor, but it has the advantage that it is a parameter which is completely independent of the model used (it depends only on the goodness of fit).

It is obvious from the figure that although strong fields are present at all flux densities [i.e. all $A(15648)$], weak fields are limited to regions with small magnetic flux densities. For $A(15648) \lesssim 0.8$ there does not appear to be a significant preference for any particular field strength. In particular there is no clustering of points close to 400G. Such a clustering is expected

330
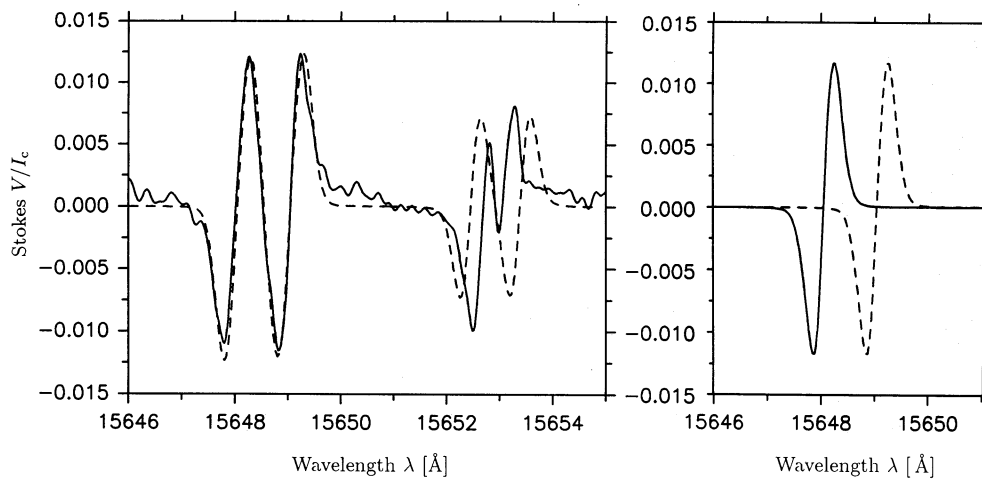
Fig. 9. Same observed spectrum as in Fig. 8a, but now fitted with $B_1(z=0) = B_2(z=0) = 900G$ and $\Delta\lambda_V = 19$km s^{-1}. Note the good fit to the $g = 3$ line although the profiles in Fig. 9b are quite different from those in Fig. 8b. Also note the bad fit to the $g_{eff} = 1.53$ line
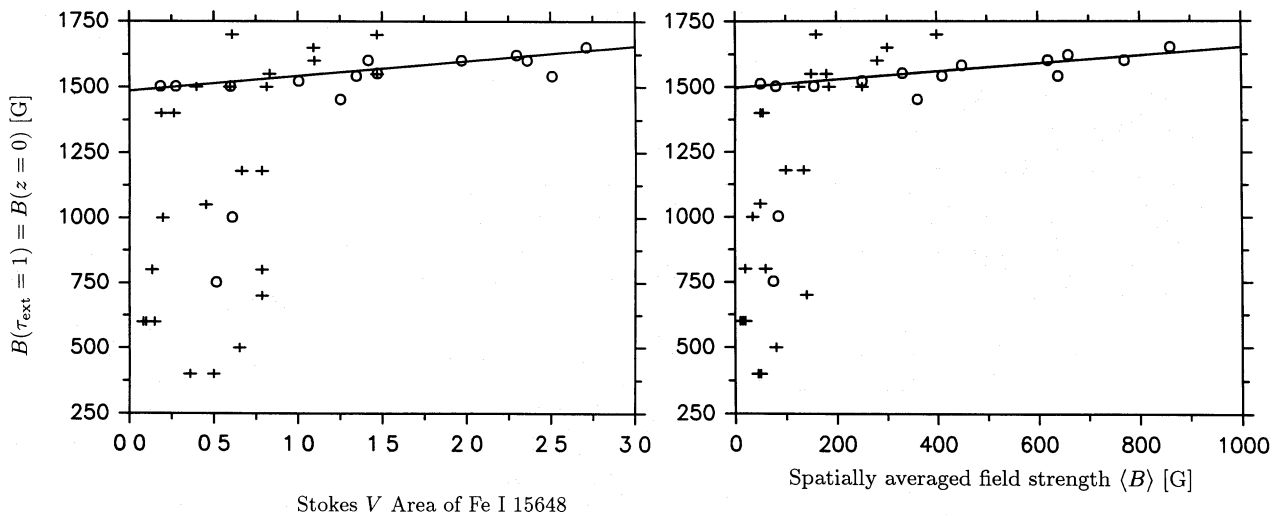
Fig. 10. a. $B(z=0)$ vs. $A(15648)$ [mÅ], the Stokes V lobe area of Fe I 15648.5Å, for all the observed regions. If more than one magnetic component is needed to fit the observed profile, then $B(z=0)$ for each component is plotted (vs. the Stokes V area belonging to that component alone). $B(z=0)$ values resulting from such 2-magnetic-component fits are denoted by a '+', while the $B(z=0)$ obtained from single components are marked by a 'o'. The solid line is a regression through all the points with $\beta \lesssim 1$, i.e. with $B(z=0) \gtrsim 1250$G. **b.** $B(z=0)$ vs. $\langle B \rangle$, the field strength averaged over the spatial resolution element. Symbols are as in Fig. 10a

if a lot of net flux were present in the form of fields weaker than 400G. However, it should be noted that for $B(z=0) < 400$G the $g = 3$ line is no longer completely split, so that V is no longer proportional to the filling factor α alone, but to αB, so that its sensitivity to detecting weaker fields is small and decreases linearly with decreasing field strength. Note that only in three out of 27 regions does B_1 lie in the weak-field regime. This is not surprising since the observations were carried out in an active plage where we generally expect to find strong fields almost everywhere.

In Fig. 10b we again plot $B(z=0)$, but this time vs. $\langle B \rangle$, the spatially averaged field strength for each magnetic component. For a fixed entrance aperture and constant seeing $\langle B \rangle$ is a measure of the amount of flux. Thus Fig. 10b is physically more meaningful than Fig. 10a, but also much more model dependent, since $\langle B \rangle$ [like the filling factor $\alpha(z=0)$] depends on the temperature structure, field inclination, etc., and is thus much more uncertain than $B(z=0)$ and $A(15648)$. Figure 10b shows the same qualitative behaviour as Fig. 10a. However, it demonstrates even more clearly that the regions with $\beta > 1$ have rather small magnetic fluxes. The $B(\tau = 1)$ values show much more scatter

than the $B(z=0)$ values, exactly as expected (see Paper II and Zayer et al. 1990).

5.3. Fluxes

Let us now consider the total fluxes in weak and strong magnetic fields, respectively. A histogram of $\langle B \rangle$ is plotted in Fig. 11 as a function of the plasma β. The dashed vertical lines at $\beta = 1.8$ is the limit for convective stability given by Spruit & Zweibel (1979), cf. Webb & Roberts (1978). Evidently most of the magnetic flux is in strong-field form. We deduce that roughly 90% of the magnetic flux in our sample is in strong-field form ($\beta < 1$). Similarly, using the Spruit & Zweibel limit we find that approximately 93% of the magnetic flux is in a form which is convectively stable. These estimates only refer to the net flux in the resolution element. The statistical uncertainty of the result (due to noise, etc.) is 2–3%. The true uncertainty is larger due to systematic effects, e.g. temperature, selection effects of our sample, etc. Furthermore, it is not possible to detect a mixed-polarity field with dominant horizontal length scales less than approximately 2″ using our
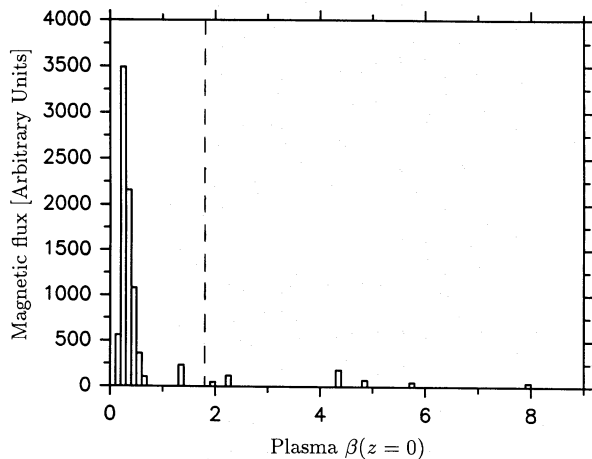
Fig. 11. Histogram of $\langle B \rangle$ vs. plasma $\beta(z = 0)$. $\langle B \rangle$ is a measure of the absolute value of the magnetic flux within the spatial resolution element as contributed by each magnetic component. The vertical dashed line at $\beta = 1.8$ marks the boundary for convective stability according to Spruit & Zweibel (1979). Two small peaks around $\beta(z = 0) = 12$ and 19 lie outside the frame

data. The uncertainty given above does not take into account any possible turbulent field.

The average weighted β of the whole sample is $\overline{\beta} = 0.87$, where

$$\overline{\beta} = \frac{\sum_i \langle B \rangle_i \beta_i}{\sum_i \langle B \rangle_i}.$$

The index i runs over all spectra and all components. The large value of $\overline{\beta}$ is misleading, since the few regions with very large β affect it by an inordinately large amount. Thus it would be wrong to conclude that the average $B(z = 0) = 1300$G. The real weighted mean B of all fields in our sample is close to 1500G. Of greater interest is to consider only the fields with $\beta < 1$. For these $\overline{\beta}(z = 0) = 0.32$ is found (corresponding to $B(z = 0) = 1580$G).

It has been argued by Frazier & Stenflo (1972), Koutchmy (1991) and Koutchmy et al. (1991) that strong-field flux tubes are associated with a weak opposite-polarity field. Their observational evidence is suggestive of return-flux, i.e. of field lines returning to the photosphere near the main flux tube (cf. Osherovich 1982). We are in a position to set upper limits on the flux in a weak ($\beta > 1$) opposite polarity field associated with strong-field magnetic elements. Such a return-flux should be visible as an oppositely polarized component in the Stokes V profile of the $g = 3$ line. If all magnetic elements have a weak opposite polarity field associated with them then it cannot contain more than approximately 5% of the total flux in strong-field form, or we would have detected it in at least 5 of our spectra now showing only a single magnetic component. If only 75% of all magnetic elements have a return flux then it can contain at the most 7–8% of the flux in the dominant polarity. Finally, if only 50% of the magnetic elements are associated with a return flux then the limit increases to approximately 15% of the flux in these magnetic features.

5.4. Filling factors

The $\alpha(z = 0)$ values in the last 2 columns of Table 1 cover a surprisingly large range. The smallest filling factors of 2–3%

testify to the sensitivity of the infrared line. The presence of very large filling factors (30–50%) confirms the results of Rabin (1992). These regions do not appear to be determined by signals from pores, since we see no sign of a lower temperature in the ratio between the two lines. Although these determinations of $\alpha(z = 0)$ are, unavoidably, relatively model dependent, they are, we believe, more reliable than filling factors determined in the visible. The 1.5 μm lines are less temperature sensitive than commonly used visible lines. In addition the continuum intensity, which affects the determined α values significantly (Grossmann-Doerth et al. 1987, Schüssler & Solanki 1988) is also less temperature sensitive at 16000Å than in the visible.

5.5. Thermodynamic parameters

The macroturbulence velocity derived from 23 out of 27 spectra is 2 km s^{-1}, which agrees well with the results of Paper I. It can be seen from Table 1 that all the Stokes V profiles can be reproduced with just two atmospheric models, the HSRASP in 21 cases and PLA in 6 cases. Hotter or cooler models gave worse fits to the ratios between the Stokes V peaks of the two lines. The predominance of the HSRASP suggests that the temperature in the lower layers of magnetic elements is lower than in recent Stokes V-based models (Solanki 1986; Keller et al. 1990a). Although it should not be given a too high emphasis, due to the low temperature sensitivity of the 1.5 μm lines (Papers I and II), this result is in good agreement with the recent analysis of Solanki & Brigljević (in preparation). Another interesting point is that if height-independent field strengths are used to fit the Stokes V profiles then even cooler models are required. The sunspot hot-component model of Obridko and Staude (1988), called OS2 (see Paper II), then becomes the most common model giving best-fit profiles. This illustrates the effect pointed out in Paper II that the ratio between the Stokes V profiles of the two lines is sensitive to the presence of a longitudinal gradient of the field.

Finally, only in 3 out of 12 complex spectra requiring fits with 2 magnetic components do we obtain a shift between the Stokes V profiles of the two components. Thus in general the gas in the weak-field component is not flowing vertically relative to that in the strong-field component. In the three cases of a shift between the two magnetic components two are downflows in the weak-field component relative to the strong field, while two solutions with opposite signs of $\Delta\lambda_V$ exist in the third case. Keeping in mind that strong fields are usually not associated with significant flows (Stenflo & Harvey 1985; Solanki 1986; Solanki & Stenflo 1986; Solanki & Pahlke 1988; Fleck 1992, Paper I) we interpret the $\Delta\lambda_V$ as downflows in the weak-field regions. Such a downflow is consistent with the expected signature of a convective collapse, but is opposite to the flow direction expected for a siphon flow between the two polarities (e.g. Thomas & Montesinos 1991; Degenhardt 1991, Paper IV).

5.6. Limits on sizes of weak-field features

By combining the measured $B(z = 0)$ and $\langle B \rangle$ with the estimated solar surface area of the spatial resolution element it is possible to determine the flux and area coverage of each component of the field in a given region. This is of particular interest for the previously unidentified weak-field patches since in this manner we set upper limits on their sizes and fluxes (if we assume that the weak-field features really do form discrete flux-tube like structures, see Sect. 8).

Table 1. Parameters derived from the fits to the 1.5 μm Stokes V profiles.

Profile No.	Model	$B(\Delta\lambda_{max})$ [G]	$B_1(z=0)$ [G]	$B_2(z=0)$ [G]	$B_1(\tau=1)$ [G]	$B_2(\tau=1)$ [G]	ξ_{mac} [km s^{-1}]	$\Delta\lambda_V$ [km s^{-1}]	β_1 $(z=0)$	β_2 $(z=0)$	$\langle B_1 \rangle$ [G]	$\langle B_2 \rangle$ [G]	$\alpha_1(z=0)$ (%)	$\alpha_2(z=0)$ (%)
1	HSRASP	1750	1600	—	2210	—	2.0	—	0.28	—	770	—	48	—
2	PLA	1800	1600	—	2260	—	2.0	—	0.29	—	620	—	39	—
3	HSRASP	1635	1540	—	2010	—	2.0	—	0.38	—	410	—	27	—
4	PLA	1690	1580	—	2190	—	2.0	—	0.32	—	450	—	28	—
5	HSRASP	1395	1450	—	1780	—	2.0	—	0.56	—	360	—	25	—
6	PLA	1425	1520	—	2000	—	2.0	—	0.42	—	250	—	16	—
7	HSRASP	1515	1500	—	1900	—	2.0	—	0.46	—	80	—	5	—
8	HSRASP	1340	1510	—	1915	—	2.0	—	0.44	—	50	—	3	—
9	PLA	2015	1650	—	2465	—	2.0	—	0.21	—	860	—	52	—
10	HSRASP	1455	1540	—	2010	—	2.0	—	0.38	—	640	—	42	—
11	HSRASP	1835	1620	—	2285	—	2.0	—	0.26	—	660	—	41	—
12	PLA	1580	1550	—	2090	—	2.0	—	0.37	—	330	—	21	—
13	PLA	1375	1500	—	1950	—	2.0	—	0.47	—	155	—	10	—
14	HSRASP	700	1000	—	1055	—	2.0	—	2.30	—	85	—	8	—
15	HSRASP	580	750	—	765	—	2.0	—	4.87	—	75	—	10	—
16	HSRASP	1220	1550	1180	2040	1295	3.5	0	0.37	1.36	180	100	12	8
17	HSRASP	1200	1600	1180	2210	1295	3.5	0	0.28	1.36	280	135	17	11
18	HSRASP	740	1000	800	1055	820	2.0	0	2.30	4.37	35	20	3	3
19	HSRASP	440	1400	400	1670	395	2.0	0	0.67	19.12	55	50	4	13
20	HSRASP	400	1500	500	1900	495	2.5	0	0.46	12.17	125	80	8	16
21	HSRASP	380	1400	400	1670	395	2.0	0	0.67	19.12	50	45	4	11
22	HSRASP	1775	1550	800	2040	820	2.0	1.4	0.37	4.37	150	60	10	7
23	HSRASP	1455	1500	−600	1900	−600	2.0	2.7	0.46	7.94	185	−13	12	3
			1500	600	1900	600	2.0	−4.1	0.46	7.94	160	10	11	2
24	HSRASP	1630	1500	−600	1900	−600	2.0	0.7	0.46	7.94	250	−13	17	2
25	HSRASP	1455	1650	−600	2430	−600	1.0	0	0.21	7.94	300	−30	18	5
26	HSRASP	double	1700	−1050	2720	−1120	2.0	0	0.14	1.95	160	−60	9	5
27	HSRASP	double	1700	−700	2720	−705	2.0	0	0.14	5.72	400	−140	24	20

Let F_{obs} denote the area of the spatial resolution element. Then we obtain an upper limit d_u on the diameter d of the weak-field magnetic features if we assume that a single magnetic feature gives rise to the whole Stokes V signal in the resolution element.

$$d(z=0) \le d_u(z=0) = 2\sqrt{\frac{\langle B \rangle F_{obs}}{\pi B}}.$$

Similarly we can obtain an upper limit Φ_u on the flux Φ within an individual weak-field magnetic element

$$\Phi \le \Phi_u = F_{obs}\langle B \rangle = \frac{\pi d_u^2}{4}B.$$

For an approximately circular spatial resolution element of 3–5″ diameter (determined mainly by seeing) we get $F_{obs} = 3 \times 10^6$–10^7km^2. From this we deduce for the two spectra with smallest $\langle B \rangle$ in weak-field form that

$$d(z=0) \lesssim 275\text{--}500\,\text{km} \quad \text{and} \quad \Phi \lesssim 4.5 \times 10^{17}\text{--}1.2 \times 10^{18}\text{Mx}.$$

The uncertainty is mainly due to the uncertain F_{obs} caused by variable seeing. In comparison, for the strong-field component we find a similar upper limit for d and $\Phi < 1.5\text{--}5 \times 10^{18}$Mx. If we assume that a weak-field patch with $d(z=0) = d_u(z=0)$ and $B(z=0) = 400$G is later concentrated to $B(z=0) = 1500$G with the same flux then we obtain

$$d_{concentrated}(z=0) \lesssim 140\text{--}250\,\text{km}.$$

6. Compatibility with visible data

In the present section we discuss the compatibility of the results obtained from the 1.5 μm lines with previous measurements of the magnetic field using lines in the visible. The most detailed such analysis is that of Zayer et al. (1990). They determine magnetic and thermodynamic parameters of 23 regions by inverting, among other Stokes V line parameters, the Stokes V ratio between Fe I 5250.2Å, Fe I 5247.1Å and Fe I 5250.6Å using flux tube models similar to ours. The 5250.2Å/5247.1Å ratio is a measure of the field strength (Stenflo 1973), while the ratio 5247.1Å/5250.6Å is a diagnostic of the temperature (Stenflo et al. 1987a). Zayer et al. found that the $B(z=0)$ derived from their data lies in the range 1450G–1700G, which is very similar to the $B(z=0)$ range of the strong-field component seen by us (see Fig. 10). However, they do not see any sign of weak fields.

We have tested the compatibility of our data set with that analysed by Zayer et al. (1990) in the following manner. We first calculate Stokes V profiles of Fe I 5250.2Å and 5247.1Å using the model parameters which best reproduce the infrared spectra. Then we form the ratio between the Stokes V amplitudes of the two lines. Finally we compare the shapes and ratios of our simulated Stokes V profiles with the visible data.

The first surprising result is that all the synthetic Stokes V profiles of the visible lines look normal and simple, i.e. none shows obvious signs of a second magnetic component. To illustrate this we show in Fig. 12 the Stokes V profiles of Fe I 5250.2Å (Figs. 12a and b) and of Fe I 5247.1Å (Figs. 12c and d) calculated using the parameters derived from spectrum No. 26. Although the 1.5 μm lines show very obvious signs of two magnetic components (Fig. 8), the composite profiles in the visible look quite normal (Figs. 12a and c). The Stokes V profiles of the individual magnetic components are plotted in Figs. 12b and d.
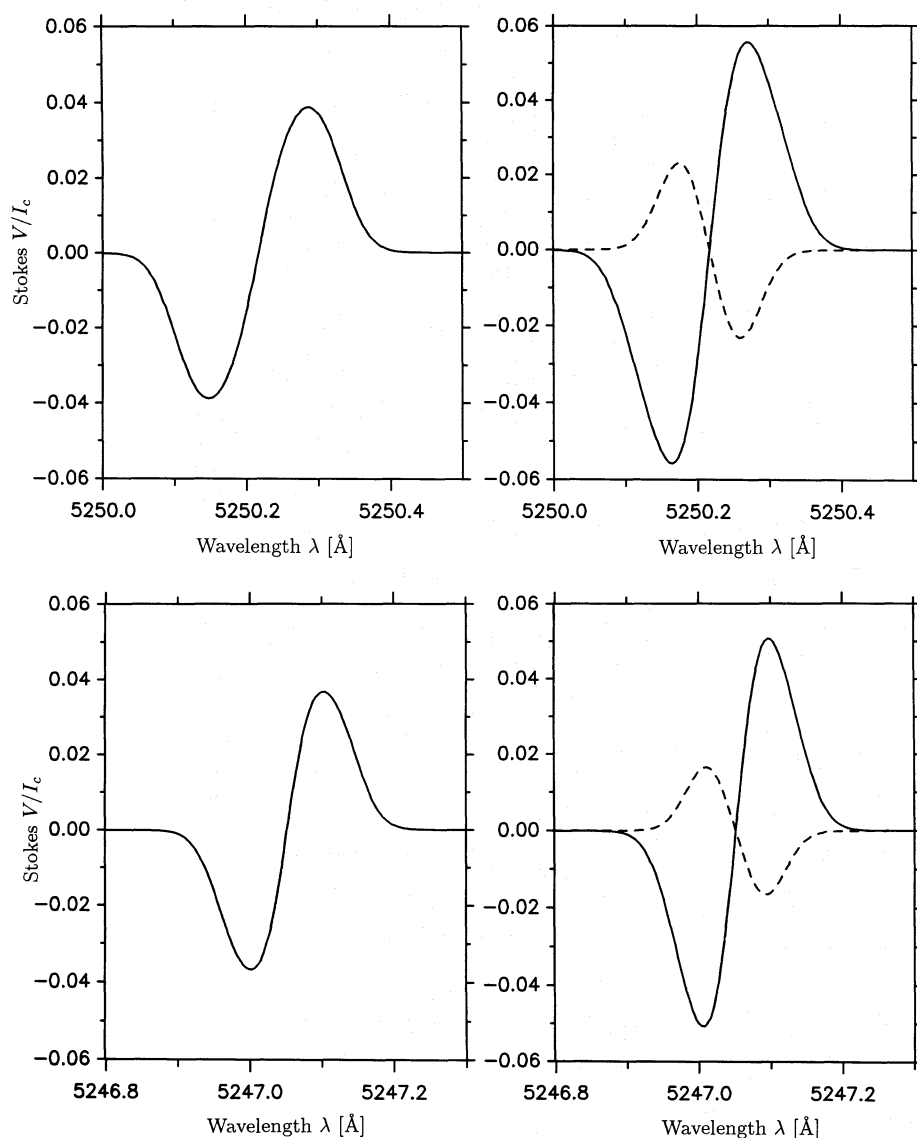
Fig. 12. a. Synthetic Stokes V profile of Fe I 5250.2Å ($g = 3$) for the same model as the dashed profile in Fig. 8a. Note the absence of an inversion in the core of λ5250.2Å. **b.** The λ5250.2Å profiles of the two individual magnetic components of which the Stokes V profile in Fig. 12a is composed. **c.** Same as Fig. 12a for Fe I 5247.1Å ($g_{\rm eff} = 2$). **d.** Same as Fig. 12b for λ5247.1Å

Note the relative weakness of the Stokes V profiles of the second magnetic component, due primarily to the lower magnetic sensitivity of 5250.2Å and 5247.1Å (the effect is enhanced by their greater heights of formation, at which B is smaller). In addition the $\xi_{\rm mac} = 2$km s^{-1} with which all visible profiles are convolved (e.g. Solanki et al. 1987) affects the narrow, weakly split minority component by a larger amount than the major component.

In Fig. 13 the line ratio formed from the Stokes V profiles of the calculated λ5250.2Å and λ5247.1Å lines are plotted vs. the net $\langle B \rangle$, defined as $\langle B_1 \rangle + \langle B_2 \rangle$, where the sign of $\langle B_2 \rangle$ is positive if the second magnetic component has the same polarity as the first magnetic component and negative if the polarities are opposite. The straight line is a regression through the strong-field single-component points (i.e. through all circles, except the two lying above a ratio of 0.95). The line ratio values corresponds to three $B(z = 0)$ (750G, 1500G and 1700G) are marked by arrows at the right of the frame.

A number of points in Fig. 13 are worthy of mention. Firstly, due to its strongly non-linear dependence on the field strength the 5250.2/5247.1 line ratio is much less suited to measure weak magnetic fields than (the direct splitting of) the 1.5 μm lines.

Secondly, the crosses show a much larger scatter than the circles. Note that the 5 crosses lying 0.05–0.1 above the regression line all represent unipolar regions, while the 3 crosses 0.1–0.15 below the regression line represent regions of mixed polarity. This is in agreement with the arguments of Semel (1986) and Solanki (1992). Whereas a mixture of fields with the same polarity gives a line ratio between that expected for the individual magnetic components, mixed polarities lead to line ratios corresponding to field strengths higher than found in either of the components.

Thirdly, a comparison with the line ratio derived from observed profiles by Stenflo & Harvey (1985) and Zayer et al. (1990) shows the following: A) The scatter in the synthetic line ratio is larger than in the measurements. B) The qualitative dependence
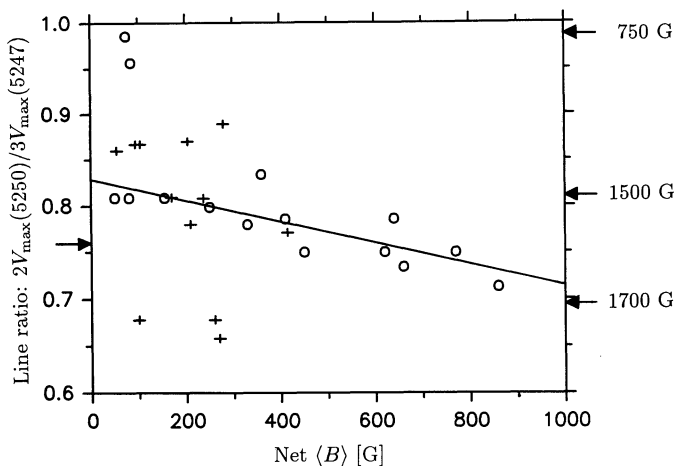
Fig. 13. Synthetic magnetic line ratio $2 \times V_{max}(5250)/(3 \times V_{max}(5247))$ expected from the analysis of the 1.5 μm lines vs. $\langle B \rangle$. Note that now the '+' signs refer to the composite profiles, including contribution from both magnetic components. The solid line is a regression through the circles with a line ratio below 0.9, i.e. all the single component strong-field data points. The arrow at the left of the frame corresponds to the average magnetic line ratio extrapolated to $V_{max} = 0$ in the data of Zayer et al. (1990)

on filling factor is the same, i.e. the line ratio decreases as V_{max} increases.[5] C) The absolute value of the synthetic line ratio is somewhat larger than that of the measured line ratio. The arrow on the left side of the frame marks the observed average line ratio extrapolated to $V_{max} = 0$. The difference between observed and synthetic line ratios is approximately 0.05, corresponding roughly to $\Delta B(z = 0) = 100$G. D) The $\langle B \rangle$ values derived from the infrared reach much larger values than those derived from visible spectra.

The obvious explanation for the difference in absolute values between the synthetic and observed line ratios is an error in the assumed temperature stratification. We know that the temperature stratifications we have used are not entirely correct. The recent results of Solanki & Brigljević (in preparation) suggest that the temperature stratification in magnetic elements is flatter than in the models we have used. Larsson et al. (1991) have shown that for a flatter temperature stratification low excitation, temperature sensitive lines like $\lambda 5250.2$Å and $\lambda 5247.1$Å are formed deeper in the atmosphere, while the heights of formation of high excitation, relatively temperature *in*sensitive lines like $\lambda 15648$Å and $\lambda 15652$Å are left almost unchanged. Thus the main effect of a flatter temperature stratification is to decrease the difference between the heights-of-formation of the 1.5 μm and visible lines. Therefore in such models the visible lines are expected to see larger B and consequently give lower line ratios, bringing them closer to the observations. Thus Fig. 13 may in some ways serve as a crude diagnostic of the temperature gradient in solar magnetic elements.

Part of the larger scatter of the synthetic line ratio compared to the observed one may be explained by the fact that the visible

---

[5] Note the difference between the definition of the magnetic filling factor used here, $\alpha(z = 0)$, and that used by Zayer et al. (1990), $\alpha(\tau_{int} = 1$. To compare the two values the values of Zayer et al. should be multiplied by factors of 1.3–1.7. Then the filling factors determined in the visible do not differ significantly from the ones we find.

observations were always made in regions carefully chosen to be monopolar. Another part may have to do with the large temperature sensitivity of $\lambda 5250.2$Å and $\lambda 5247.1$Å. Since the 1.5 μm lines are not very temperature sensitive we have only a rough idea of the temperature in the magnetic features of the individual regions. In particular little can be said about the variation of the temperature from one region to another. Now, Zayer et al. (1990) discovered that in magnetic elements B and temperature are related in such a way that $\lambda 5250.2$Å and $\lambda 5247.1$Å always see almost the same field strength at their (temperature dependent) height of formation. If the proper temperature variation is not taken into account when calculating synthetic line ratios, then it does not compensate for the effects of the field strength to the same extent, and the scatter in the synthetic line ratio becomes larger.

7. Comparison with data obtained by the Near Infrared Magnetograph

The Near Infrared Magnetograph (NIM) has an infrared array detector system and also measures the Stokes V profiles of the $\lambda 15648$Å and $\lambda 15652$Å lines, from which in principle the same magnetic and thermodynamic parameters can be determined as in the present analysis. The instrument has been described by Rabin et al. (1991), while plage data taken with it are analysed by Rabin (1992) and in Paper IV. The main advantages of the NIM compared to the "Baboquivari" data analysed here are that all wavelengths are measured simultaneously and that information on the spatial distribution of the field in one direction is also obtained. It is gratifying to see that the Stokes V profiles obtained with the NIM can be as complex in shape as the ones analysed here and that they can be explained by 2-magnetic-component models similar to the ones used here (Paper IV). This implies that in general the complex profiles in our data are not produced by a shift in the field of view during a spectral scan (in agreement with other indicators, e.g. consistency between the two spectral lines, symmetry properties of Stokes V). However, the fraction of complex line profiles measured with the NIM is much smaller than in the present data set. Although we cannot rule out that it is partly a selection effect, it is at least to a large part due to the difference in spectral resolution between the two data sets.

The observations analysed here have an effective resolving power of approximately 150 000. This is adequate to measure field strengths down to 400–500G, which is close to the limit expected from theoretical test calculations for the $g = 3$ line (Paper II). By contrast the spectral resolving power of the present version of the NIM is only of the order of 45 000 (Paper IV), which unfortunately greatly limits its ability to detect weak fields. We estimate that the lowest $B(z = 0)$ detectable with the NIM is approximately 800–900G, i.e. approximately twice as high as the smallest values obtainable from our data. In addition a lower spectral resolution also significantly reduces the number of complex Stokes V profiles. The instrumental smearing simply wipes out the smaller features in the Stokes V profiles. To illustrate this point we show in Fig. 14a spectrum No. 25 of our data set which exhibits obvious signs of two opposite-polarity magnetic components (solid curve, cf. Fig. 7) and the same spectrum degraded to the spectral resolution of the NIM (assuming a Gaussian instrumental profile, dashed curve). No obvious sign of the second magnetic component is left and such a profile would be classified as "simple". Only in regions in which Stokes V profiles of both
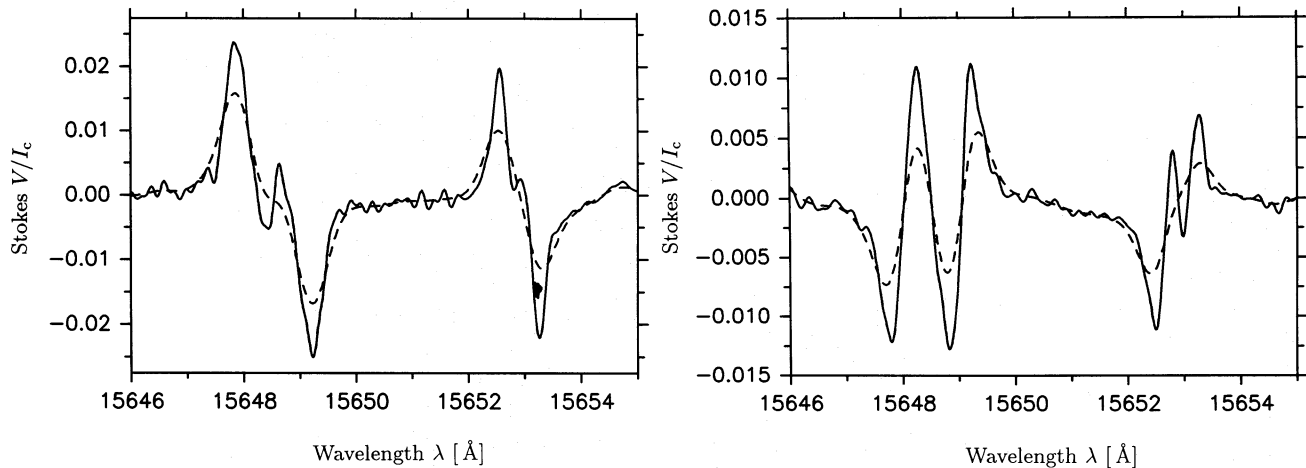
Fig. 14. Profiles as observed (solid) and after spectral smearing by an amount corresponding to the width of the apparatus function of the Near Infrared Magnetograph (dashed). **a.** Same observed profile as in Fig. 7a. **b.** Same observed profile as in Fig. 8a

magnetic components give almost equally strong Stokes V profiles are the two magnetic components still visible after spectral degradation. In our sample we find that only 2 spectra are still obviously complex after spectral degradation to the NIM value. One of these (No. 26, compare with Fig. 8) is plotted in Fig. 14b. The g=3 line survives the spectral smearing qualitatively unchanged, but the second magnetic component is no longer visible in the smeared profile of the $g_{eff} = 1.53$ line.

The field strengths measured by Rabin (1992) are closer to the B values derived directly from the splitting (column 3 of Table 1). They are, on the whole relatively similar, although field strengths below 700–800G are missing in the NIM data, of course.

The observation that strong fields occur over the whole measured range of fluxes, while weaker fields are limited to regions of small magnetic flux is in good agreement with the results of Rabin (1992, see his Fig. 11). Our measured filling factors also agree well with the values derived by Rabin (1992), although our largest α values are smaller than his by over 10%.

8. Discussion and conclusions

8.1. Summary of the results

In the present paper we have applied the diagnostics developed by Zayer et al. (1989) and in Paper II to 27 Stokes V spectra of solar plages. Using the 1.5 μm lines at λ15648Å and λ15652Å we have measured magnetic field strengths between 400G and 1700G at $z = 0$ in active region plages with an accuracy of up to 2–3%. The $B(z = 0)$ for the strong-field components agree very well with the results of Zayer et al. (1990), derived from model fits to visible data (5250.2/5247.1 line ratio). Thus, for kG fields with a simple geometry the present investigation confirms the accuracy of the line-ratio technique of Stenflo (1973). However, the visible data showed no sign of intrinsically weak fields, in contrast to the infrared data. On the other hand, much better temperature diagnostics are available in the visible, so that the formation heights and therefore B at a fixed height are better constrained by visible data. The absence of sensitive temperature diagnostics near 1.5μm is one of the main shortcomings of this wavelength band.

We estimate that the fraction of net magnetic flux in strong-field form ($\beta(z = 0) \leq 1$, i.e. $B(z = 0) \gtrsim 1250$G) is close to 90%

when observed at a spatial resolution of a couple of arc sec. We stress that the spatially averaged flux density is less reliably determined than B. This fraction is surprisingly similar to the limit set by Howard & Stenflo (1972) and Frazier & Stenflo (1972), based on visible magnetograph data. Note, however, the difference between the two results. Whereas Howard & Stenflo (1972) and Frazier & Stenflo (1972) find that 90% is a lower limit to the amount of strong-field flux (they have little conclusive evidence for the actual presence of a weak field), in our data 10% of the net flux is in weak-field ($\lesssim 1250$G) form.

The fact that 90% of the magnetic flux is in strong field form (1400G $\lesssim B(z = 0) \lesssim 1700$G) supports the view that the small-scale magnetic fields are concentrated very efficiently by e.g. the convective collapse process (Parker 1978; Hasan 1985, cf. Schüssler 1990). Spruit (1979) predicts field strengths in the interval 1280G $\lesssim B(z = 0) \lesssim 1650$G, which agrees remarkably well with the measured values.

On the other hand, our data clearly contradict the claims of Zirin & Popp (1989), based on the 12 μm lines, that there is at the most indirect evidence for kG fields in solar plages. Their interpretation of their 12 μm spectra and in particular their extrapolation of the measured field strengths to the lower photosphere is obviously flawed. See Carlsson et al. (1992) for a discussion of some of the shortcomings of the Zirin & Popp paper. Here we only wish to point out that, due to the exponential decay of B with height, a field strength of 200–400G in the upper photosphere, where the 12 μm lines are formed (e.g. Carlsson et al. 1992) is compatible with a $B(z = 0) \approx 1400$–1700G. Our results also contradict the large fraction of weak-field flux reported by Del Toro et al. (1990). They find that 57–84% of the magnetic flux is in weak field form (we cannot give an exact limit, since they do not determine $B(z = 0)$, but 57% of their flux has $B < 850$G). Although their spatial resolution is higher, our data should still allow us to detect most of the weak fields seen by them, due to our superiour "Zeeman resolution". For a critical discussion of the technique used by Del Toro et al. (1990) see Solanki (1992).

Can weak fields have escaped detection in the present investigation? We can conceive of two ways in which significant amounts ($> 5\%$) of the total magnetic flux can have escaped detection. Firstly, if the field is highly inclined then it will not be visible in Stokes V near solar disk centre. Schüssler (1990) has argued that flux tubes with lower field strengths can be easily

inclined by external flows due to their lower buoyancy. Future observations of Stokes Q and U of the 1.5 μm lines should be able to constrain such weak, inclined fields as well. A similar study in the visible by Stenflo (1988) has already set some constraints, but it should be possible to achieve a much higher sensitivity in the infrared. Another way for weak fields to escape detection is if they change polarity on a short horizontal scale ($\lesssim$ 2–3″) and if both polarities have similar field strengths. To detect such a mixed-polarity or turbulent field, Stokes V spectra at 1.5 μm with higher spatial resolution are required.

The analysis of the present data set has confirmed the main advantages of measuring magnetic field strengths in solar plages using the 1.5 μm $g = 3$ line (see also Paper II). It has the capability of measuring kG fields very simply and with high accuracy and of detecting and measuring weak fields down to $B(z = 0) \approx 400$G (in the thin-tube approximation). It is relatively temperature insensitive, so that more accurate filling factors can be determined. Its large Zeeman sensitivity allows it to separate multiple components of the field strength within the spatial resolution element.

To make full use of the potential of this line the observations must have a high spectral resolution of at least 100 000 (to obtain a high Zeeman resolution) and a S/N ratio higher than approximately 10^3 in the continuum (to detect features with small fluxes and to obtain Stokes V profile shape information reliably).

What is the nature of the observed weak-field features? We envisage the following three possibilites: 1. The weak fields are associated directly with the strong fields, e.g. in the form of return flux or of a thick transition layer of the flux tubes. 2. They are part of the superpenumbral canopy of sunspots (see Paper V). 3. They form independent patches of magnetic flux and possibly are associated with intranetwork fields (Livingston & Harvey 1971).

Possibility 1 appears unlikely, since we see weak fields in only half the analysed regions. In addition, where a weak and a strong field are present they usually form two quite distinct magnetic components, so that the weak fields cannot be part of an extensive transition layer separating strong fields from the field-free gas. Another strong piece of evidence against the direct association of the observed weak fields with strong-field flux tubes is that in three regions we find only weak fields, with no sign of any strong field at all. At least these fields cannot be associated with stronger fields.

We cannot rule out that at least some of the observed weak fields are simply the signature of the superpenumbral canopy of sunspots embedded in the observed plages. Solanki et al. (1992b, Paper V of the present series) show that the signal of the superpenumbral canopy can be seen in the $g = 3$ line even 20 arc sec away from one particular sunspot. For more details see Paper V.

Consider now the third explanation, namely that the $\beta > 1$ features represent isolated patches of magnetic flux. It is likely that at least some of them have this physical background. What can we say about their properties? Approximately 11% of the total flux is in a form with $\beta > 1$, and 8% has $\beta \gtrsim 2$. Thus most of the weak field is in a convectively unstable form. On the other hand, the measured field strengths are sufficiently large for the magnetic energy of the weak fields to be larger than with the kinetic energy of the convective velocity field. Thus the weak fields have already been partially concentrated by the flux expulsion process (Parker 1963; Weiss 1966; Galloway & Weiss 1981; Nordlund 1983). There are two scenarios for the production of such weak-field flux. i) It is relatively freshly emerged field which either appeared at this strength from the solar interior or

has been swept together to this strength by the granulation, but has not yet undergone convective collapse. ii) It is the product of the decay of strong-field flux tubes into weaker fields (e.g. Spruit et al. 1992) by either fragmentation to very small flux tubes or reconnection below the surface to form U shaped loops. It may be possible to distinguish between the two scenarios by considering other properties of the weak fields.

The smallest upper limit on the sizes of weak-field patches, 275–500km is unfortunately too large to distinguish between the scenarios. On the other hand, the relative lack of flows in the weak magnetic patches relative to the strong ones (only 3 out of 11 regions show such a flow) implies that the gas in the weak field patches is relatively static. This in turn implies that these patches are neither undergoing convective collapse (which would produce a downflow), nor do they contain a siphon flow (which would produce an upflow). Since these are the two main mechanisms which have been proposed for the concentration of photospheric magnetic fields (e.g. Thomas 1990), this observation suggests that the weak fields are mainly in a stable form. The only relatively stable forms of the weak field are very small flux tubes, for which horizontal radiative exchange suppresses convective collapse (Venkatakrishnan 1986, Schüssler 1990) and U loops, which cannot undergo convective collapse since matter cannot flow down (Spruit et al. 1987). Our observations therefore support the existence of such structures.

Are the weak-field patches related to the intranetwork field? Our observations do not allow us to decide this question (the fluxes we measure are an order of magnitude larger than the estimate, $\approx 5 \times 10^{16}$Mx, for the typical flux in a single intranetwork element (made by Harvey 1977). Note that the weak fields found here were all seen in active region plages. Therefore, if they are related to intranetwork fields, they should be found everywhere on the sun.

In at least 2 out of 3 weak-field patches showing flows, the flows are directed downwards, while in the third the direction of the flow is not certain. This suggests that convective collapse is more important than siphon flows (which produces upwards directed flows in the weak field) as a mechanism for flux concentration. However, we stress that the number of spectra on which this conclusion is based is *very* small. Much better statistics are required before definitive conclusions can be drawn. The above argument only illustrates another aspect of the 1.5 μm lines as diagnostics of the physics of solar magnetic features.

Finally, let us turn the question around and ask: Can we set limits on the amount of weak-field flux associated with strong fields? We cannot rule out the presence of a smooth transition layer of, say, 10–20% of the flux tube width. Flux tubes with a very sharp boundary and tubes with a more extended boundary give relatively similar Stokes V profile shapes if $B(z = 0)$ of the latter is increased by an appropriate amount (approximately 20–50G).

The fact that the number of weak-field patches with a polarity opposite to that of the strong field is smaller than the number of spectra in which the weak field has the same polarity as the strong field speaks against the general presence of return flux around small flux tubes. The possibility of such a return flux had been hypothesized by Frazier & Stenflo (1972) and by Zayer et al. (1989). The present observations show that the weak, opposite polarity field in the profile observed by Zayer et al. (1989) is not typical for the $g = 3$ line. Evidence for the almost universal presence of an opposite polarity field around small-scale magnetic features has been presented by Koutchmy (1991) and Koutchmy

et al. (1991). One theoretical description of such opposite polarity fields is based on return-flux models (e.g. Osherovich 1982). If such return flux is practically universal then in order to be compatible with our data it cannot contain more than 5% of the flux of the dominant polarity. Therefore, either the fluxes observed by Koutchmy (1991) and Koutchmy et al. (1991) are below this limit, and thus of little consequence for the magnetic and thermodynamic structure of the solar atmosphere, or else we must look into alternative explanations of their observations (e.g. small loops or the proposal of Harvey 1991).

References

Brault J.W., Noyes R.W., 1983, ApJ 269, L61

Bruls J.H.M.J., Solanki S.K., 1992, A&A to be submitted

Carlsson M., Rutten R.J., Shchukina N.G., 1992, A&A 253, 567

Degenhardt D., 1991, A&A 248, 637

Deinzer W., Hensler G., Schüssler M., Weisshaar E., 1984, A&A 139, 435

Del Toro Iniesta J.C., Semel M., Collados M., Sánchez Almeida J., 1990, A&A 227, 591

Deming D., Boyle R.J., Jennings D.E., Wiedemann G., 1988, ApJ 333, 978

Fleck B., 1991, Rev. Modern Astron. 4, 90

Frazier E.N., Stenflo J.O., 1972, Sol. Phys. 27, 330

Frazier E.N., Stenflo J.O., 1978, A&A 70, 789

Galloway D.J., Weiss N.O., 1981, ApJ 243, 945

Grossmann-Doerth U., Pahlke K.-D., Schüssler M., 1987, A&A 176, 139

Grossmann-Doerth U., Schüssler M., Solanki S.K., 1989, A&A 221, 338

Harvey J.W, 1977, in Highlights of Astronomy, E.A. Müller (Ed.), Vol. 4, Part II, p. 223

Harvey J.W., 1991, in Solar Polarimetry, L.J. November (Ed.), National Solar Obs., Sunspot, p. 250

Harvey J.W., Hall D., 1975, BAAS 7, 459

Hasan S.S., 1985, A&A 143, 39

Howard R.W., Stenflo J.O., 1972, Sol. Phys. 22, 402

Illing R.M.E., Landman D.A., Mickey D.L., 1975, A&A 41, 183

Keller C.U., Solanki S.K., Steiner O., Stenflo J.O., 1990a, A&A 233, 583

Keller C.U., Solanki S.K., Tarbell T.D., Title A.M., Stenflo J.O., 1990, A&A 236, 250

Koutchmy S., 1991, in Solar Polarimetry, L. November (Ed.), National Solar Obs., Sunspot, NM, p. 237

Koutchmy S., Zirker J.B., Darvann T., Koutchmy O., Stauffer F., Mann R., Coulter R., Hegwer S., 1991, in Solar Polarimetry, L. November (Ed.), National Solar Observatory, Sunspot, NM, p. 263

Larsson B., Solanki S.K., Grossmann-Doerth U., 1991, in Solar Polarimetry, L. November (Ed.), National Solar Obs., Sunspot, NM, p. 479

Lites B.W., Skumanich A., Rees D.A., Murphy G.A., Carlsson M., 1987, ApJ 318, 930

Livingston W., 1991, in Solar Polarimetry, L. November (Ed.), National Solar Obs., Sunspot, NM, p. 356

Livingston W., Harvey J.W., 1971, in Solar Magnetic Fields, R. Howard (Ed.), , IAU Symp. 43, 51

Martin S.F., 1988, Sol. Phys. 117, 243

Mathys G., 1988, A&A 189, 179 Recorded in Circularly Polarized Light.

Muglach K., Solanki S.K., 1992, A&A 263, 301 (Paper I)

Nordlund Å., 1983, in Solar and Stellar Magnetic Fields: Origins and Coronal Effects, J.O. Stenflo (Ed.), Reidel, Dordrecht, IAU Symp. 102, 79

November L.J., 1991, in Solar Polarimetry, L.J. November (Ed.), National Solar Obs., Sunspot, NM, p. 149

Obridko V.N., Staude J., 1988, A&A 189, 232

Osherovich V.A., 1982, Sol. Phys. 77, 63

Parker E.N., 1963, ApJ 138, 552

Parker E.N., 1978, ApJ 221, 368

Rabin D., 1992, ApJ 391, 832

Rabin D., Jaksha D., Plymate C., Wagner J., Iwata K., 1991, in Solar Polarimetry, L. November (Ed.), National Solar Observatory, Sunspot, NM, p. 361

Rüedi I., 1991, Diplomarbeit, ETH, Zürich

Rüedi I., Solanki S.K., Rabin D., 1992, A&A 261, L21 (Paper IV)

Schüssler M., 1990, in Solar Photosphere: Structure, Convection and Magnetic Fields, J.O. Stenflo (Ed.), Kluwer, Dordrecht, IAU Symp. 138 161

Schüssler M., Solanki S.K., 1988, A&A 192, 338

Semel M., 1986, in Small Scale Magnetic Flux Concentrations in the Solar Photosphere, W. Deinzer, M. Knölker, H.H. Voigt (Eds.), Vandenhoeck & Ruprecht, Göttingen, p. 39

Skumanich A., Lites B.W., 1991, in Solar Polarimetry, L. November (Ed.), National Solar Observatory, Sunspot, NM, p. 307

Solanki S.K., 1986, A&A 168, 311

Solanki S.K., 1990, in Solar Photosphere: Structure, Convection and Magnetic Fields, J.O Stenflo (Ed.), Kluwer, Dordrecht, IAU Symp. 138, 103

Solanki S.K., 1992, Space Sci. Rev. to be submitted

Solanki S.K., Keller C., Stenflo J.O., 1987, A&A 188, 183

Solanki S.K., Pahlke K.D., 1988, A&A 201, 143

Solanki S.K., Rüedi I., Livingston W., 1992a, A&A 263, 312 (Paper II)

Solanki S.K., Rüedi I., Livingston W., 1992b, A&A 263, 339 (Paper V)

Solanki S.K., Rüedi I., Livingston W., Stenflo J.O., 1992c, in Cool Stars, Stellar Systems and the Sun, VII, J. Bookbinder, M. Giampapa (Eds.), in press

Solanki S.K., Stenflo J.O., 1984, A&A 140, 185

Solanki S.K., Stenflo J.O., 1985, A&A 148, 123

Solanki S.K., Stenflo J.O., 1986, A&A 170, 120

Spruit H.C., 1976, Sol. Phys. 50, 269

Spruit H.C., 1979, Sol. Phys. 61, 363

Spruit H.C., Schüssler M., Solanki S.K., 1992, in Solar Interior and Atmosphere, A.N. Cox, W. Livingston, M.S. Matthews (Eds.), University of Arizona press, Tucson, p. 890

Spruit H.C., Van Ballegooijen A.A., Title A.M., 1987, Sol. Phys. 110, 115

Spruit H.C., Zweibel E.G., 1979, Sol. Phys. 62, 15

Steiner O., Pneuman G.W., Stenflo J.O., 1986, A&A 170, 126

Stenflo J.O., 1973, Sol. Phys. 32, 41

Stenflo J.O., 1982, Sol. Phys. 80, 209

Stenflo J.O., 1988, Sol. Phys. 114, 1

Stenflo J.O., 1989, A&AR 1, 3

Stenflo J.O., Harvey J.W., 1985, Sol. Phys. 95, 99

Stenflo J.O., Solanki S.K., Harvey J.W., 1987a, A& A 171, 305

Stenflo J.O., Solanki S.K., Harvey J.W., 1987b, A& A 173, 167

Tarbell T.D., Title A.M., 1977, Sol. Phys. 52, 13

Thomas J.H., 1990, in Physics of Magnetic Flux Ropes, C.T. Russell, E.R. Priest, L.C. Lee (Eds.), Geophysical Monograph 58, American Geophys. Union, Washington, DC, p. 133

Thomas J.H., Montesinos B., 1991, ApJ 375, 404

Venkatakrishnan P., 1986, Nat. 322, 156

Webb A.R., Roberts B., 1978, Sol. Phys. 59, 249

Weiss N.O., 1966, Proc. Roy. Soc. London, Ser.A 293, 310

Wiehr E., 1978, A& A 69, 279

Zayer I., Solanki S.K., Stenflo J.O., 1989, A& A 211, 463

Zayer I., Solanki S.K., Stenflo J.O., Keller C.U., 1990, A& A 239, 356

Zirin H., 1988, Astrophysics of the Sun, Cambridge University Press, Cambridge

Zirin H., Popp B., 1989, ApJ 340, 571